

Modeling the Heart as a Communication System

Hiroshi Ashikaga^{1*}, José Aguilar-Rodríguez^{2,3}, Shai Gorsky⁴, Elizabeth Lusczek⁵, Flávia Maria Darcie Marquitti⁶, Brian Thompson⁷, Degang Wu⁸, Joshua Garland⁹

1 Division of Cardiology, Johns Hopkins University School of Medicine, Baltimore, MD, USA

2 Institute of Evolutionary Biology and Environmental Studies, University of Zurich, Switzerland

3 Swiss Institute of Bioinformatics, Lausanne, Switzerland

4 Department of Economics, University of Utah, Salt Lake City, UT, USA

5 Department of Surgery, University of Minnesota, Minneapolis, MN, USA

6 Departamento de Ecologia, Universidade de São Paulo, Brazil

7 Network Science Division, US Army Research Laboratory, Adelphi, MD, USA

8 Department of Physics, The Hong Kong University of Science and Technology, Clear Water Bay, Hong Kong, HKSAR, China

9 Department of Computer Science, University of Colorado, Boulder, CO, USA

*E-mail: hashika1@jhmi.edu

Summary

Electrical communication between cardiomyocytes can be perturbed during arrhythmia, but these perturbations are not captured by conventional electrocardiographic metrics. We developed a theoretical framework to quantify electrical communication using information theory metrics in 2-dimensional cell lattice models of cardiac excitation propagation. The time series generated by each cell was coarse-grained to 1 when excited or 0 when resting. The Shannon entropy for each cell was calculated from the time series during four clinically important heart rhythms: normal heartbeat, anatomical reentry, spiral reentry, and multiple reentry. We also used mutual information to perform spatial profiling of communication during these cardiac arrhythmias. We found that information sharing between cells was spatially heterogeneous. In addition, cardiac arrhythmia significantly impacted information sharing within the heart. Entropy localized the path of the drifting core of spiral reentry, which could be an optimal target of therapeutic ablation. We conclude that information theory metrics can quantitatively assess electrical communication among cardiomyocytes. The traditional concept of the heart as a functional syncytium sharing electrical information cannot predict altered entropy and information sharing during complex arrhythmia. Information theory metrics may find clinical application in the identification of rhythm-specific treatments which are currently unmet by traditional electrocardiographic techniques.

Key Index Words

Information Theory; Cardiac Electrophysiology; Cardiac Arrhythmia; Mathematical Modeling

Introduction

The human heart consists of 5 billion autonomous cardiomyocytes [1] with simple rules of operation and minimal central control. The behaviors of individual cardiomyocytes are orchestrated by electrical conduction between adjacent cells connected by specialized cell-to-cell junctions called intercalated discs [2]. The intercalated discs contain gap junctions with large nonselective connexin channels that allow ions and other small molecules to diffuse freely in the cytosol of adjacent cells and reduce internal electrical resistance [3]. By providing low-resistance connections between cardiomyocytes, gap junction channels allow electrical waves to propagate rapidly throughout the heart [4]. However, this task can be perturbed during cardiac arrhythmia (abnormal heart rhythm). Normally functioning cardiomyocytes can not only interrupt the electrical information flow at a wavebreak [5], they can also generate a completely different output by creating a reentry circuit where the wave rotates around the wavebreak. Arrhythmia can result from a wavebreak in an intersection between a wavefront and a wavetail [6], which leads to loss of information about the input.

Conventional electrocardiographic metrics can measure the sequence of electrical excitation [7–9], but cannot quantify how arrhythmia impacts the communication between individual cardiomyocytes. In contrast, information theory metrics such as mutual information can quantify the sharing of information in the presence of arrhythmia. Information theory has been used to evaluate biological communication in computational neuroscience [10], transcriptional regulation [11, 12], bacterial quorum sensing [13], chemotaxis [14], biochemical signaling networks [15], and evolutionary biology [16]. We propose a novel application of information theory to analyze the cardiac electrical communication system (Figure 1A).

We propose that electrical wave propagation is the mechanism by which information is shared between cardiomyocytes in the whole heart. Under this paradigm, heart rhythm disorders result from abnormal production and transmission of information that can be quantified by information theory measures. To this end, we developed a framework to quantify cardiac electrical communication during action potential propagation in normal and abnormal heart rhythms. Three major mechanisms of clinically important arrhythmias that could lead to sudden death were considered: anatomical reentry (reentry around an anatomically defined circuit [17]), spiral reentry (functional reentry without an anatomically defined circuit [18]), and multiple reentry (multiple functional reentry circuits in the presence of ongoing wavebreak [19]).

Materials and Methods

Models of Action Potential Propagation

To develop the information theory framework, we employed two commonly used mathematical models of cardiac action potential propagation. The first model was a monodomain reaction diffusion (RD) model that was originally derived by FitzHugh [20] and Nagumo [21] as a simplification of the biophysically based Hodgkin-Huxley equations describing current carrying properties of nerve membranes [22] which was later modified by Rogers and McCulloch to represent cardiac action potential [23]. This model reproduces several physiological properties known to be important in arrhythmogenesis including slowed conduction velocity (CV) and unidirectional block due to wavefront curvature [23]. This model was used widely in previous studies [24–30].

$$\frac{\partial v}{\partial t} = 0.26v(v - 0.13)(1 - v) - 0.1vr + I_{ex} + G_x \frac{\partial^2 v}{\partial x^2} + G_y \frac{\partial^2 v}{\partial y^2} \quad (1)$$

$$\frac{\partial r}{\partial t} = 0.013(v - r) \quad (2)$$

Here, v is the excitation variable which can be identified with transmembrane potential, r is the recovery variable, I_{ex} is the external current [5], and G_x and G_y are the conductance in x and y directions on the lattice, respectively. In this study the lattice was assumed to be isotropic (i.e., $G_x = G_y$). The model equations were solved using a finite difference method for spatial derivatives and explicit Euler integration for time derivatives assuming Neumann boundary conditions.

Cellular automata (CA) models have been used to study cardiac action potential propagation in several previous studies [31–40]. The model we used employed realistic restitution properties and the curvature phenomenon [41]. Each cell can adopt one of the following three physiologically meaningful states: resting, refractory₁ and refractory₂. Cells in the resting state are relaxed and can be excited while cells in both refractory states are excited. Cells in refractory₁ can excite neighboring cells, while cells in refractory₂ cannot. The depolarization (or excitation) of a cell is the transition from the resting state into the refractory₁ state and occurs according to a probabilistic update rule P^{exc} based on two influences: (1) the intrinsic cell excitability (E) that increases with the time of a cell at rest, and (2) the amount of excitation in the neighborhood of a cell (Q):

$$P_j^{exc} = EQ = E \sum_{i \neq j} \frac{A_i}{d_{ij}^2} \quad (3)$$

where i is a cell adjacent to j , A_i is a binary excitation state with a value of 0 for the resting state and a value of 1 for either of the two refractory states, and d_{ij} is the distance between the midpoints of cells i and j . E was estimated using the restitution curve of the CV , which depends on the duration of the previous diastolic interval (DI). The transitions from refractory₁ to refractory₂ (partial repolarization) and from refractory₂ to resting (total repolarization) are deterministic. The total time spent in the two refractory states matches the total action potential duration (APD). The period in the refractory₁ state is equal to 10% of the APD . The APD was estimated based on the restitution curve of the APD , which is also a function of the duration of the preceding DI . In addition to APD and CV restitution properties, Equation 3 also reproduces CV slowing in areas with a pronounced wavefront curvature because of the decreased probability of excitation. The action potential was reproduced according to the Luo-Rudy model [42], which associates the time for which each cell has been in its current state with its voltage level.

For both models, the cardiac tissue was simulated as a 2-dimensional (2-D) 128×128 isotropic lattice of cells (Figure 1B). In each cell, the time series of cardiac excitation was computed for 10 seconds with a discrete sampling rate of 500/sec (temporal resolution $\Delta t=2$ ms, Figure 1C). The duration and the sampling rate of the time series were determined to reflect realistic measurements in human clinical electrophysiology studies [43].

Cardiac Simulation

We simulated four different heart rhythms in both the RD and CA models: normal heartbeat, anatomical reentry, spiral reentry, and multiple reentry. The latter two are considered to be important mechanisms of cardiac fibrillation, including atrial fibrillation (AF) and ventricular fibrillation (VF) [18, 19]. Cardiac simulation was performed using MATLAB R2014a (Mathworks, Inc.).

Normal heartbeat was simulated as regular point stimulations (60 beats/min) originating from the top middle region of the lattice. This pattern of stimulation caused a regular train of curved excitation wavefronts traveling from top to bottom along the vertical axis in both the RD (Video S1) and CA models (Video S2).

Anatomical reentry is characterized by an electrical wavefront that travels along a preformed anatomical obstacle, most commonly a scar resulting from healed myocardial infarction, and re-excites previously excited tissue. We simulated a cardiac impulse which can rotate around the obstacle, leading to repetitive, rapid excitation of the heart. Anatomical reentry was reproduced in the RD (Video S3) and the

CA models (Video S4) by simulating a non-excitable circular region in the center of the lattice occupying 20% of the total surface area.

For spiral reentry [18], we simulated a 2-D wave of excitation emitted by an organizing source (or ‘rotor’) of functional reentry whose front is an involute spiral with increasing convex curvature toward the rotation center [44]. The spiral reentry was generated by a cross-field stimulation protocol [5] in both the RD (Video S5) and the CA models (Video S6).

Multiple reentry is characterized by multiple independent circuits of functional reentry occurring simultaneously and propagating randomly throughout the cardiac tissue [45]. Wavefronts continuously undergo wavefront-wavetail interactions resulting in wavebreak and generation of new wavefronts [46]. Multiple reentry was reproduced in the RD (Video S7) and the CA models (Video S8) by a train of random point stimulations in the substrate where the APD is shortened by 40%.

Information Measures

For each cell, the time series of cardiac excitation was coarse-grained to one when excited (during the APD at 90% repolarization, or APD_{90}) or zero when resting (Figure 1C). We treated each cell on the lattice as a time-series process X where at any observation time t the process X is either excited or resting, in which case we define $X_t = 1$ or $X_t = 0$, respectively.

Using this framework, we can compute the Shannon entropy H of each time-series process X :

$$H(X) = - \sum_x p(x) \log_2 p(x) \quad (4)$$

where $p(x)$ denotes the probability density function of the time series generated by X . This quantifies the average uncertainty of whether a single cell is excited or resting over each cell’s time history [47].

Mutual information $I(X; Y)$ is a measure of the reduction in uncertainty of the time-series process X due to the information gained from knowing the time-series process Y ; hence, this quantity is commonly viewed as the information shared between X and Y [47]. Therefore, by computing the mutual information, we can receive insight into which cells share information and how much. Formally, the mutual information between the time-series processes, in this case cells, X and Y is:

$$I(X; Y) = \sum_{x,y} p(x, y) \log_2 \frac{p(x, y)}{p(x)p(y)} \quad (5)$$

$$= H(X) + H(Y) - H(X, Y) \quad (6)$$

where $p(x, y)$ and $H(X, Y)$ denote the joint probability density function and the joint entropy of X and Y , respectively (Figure 1A).

To understand the spatial profiles of information sharing between cardiomyocytes, mutual information was computed between each of five representative cells (green circles in (Figure 1D) and all other cells in the 2-D lattice taken individually. These representative cells were defined to be in the left-upper quadrant (32, 32), the right-upper quadrant (32, 96), the center (64, 64), the left-lower quadrant (96, 32), and the right-lower quadrant (96, 96). These points were chosen to avoid artifacts generated by the boundary conditions and point stimulation in the RD model as discussed in the *Results* section. Custom programs in Python were used to compute information measures.

Results

Normal Heartbeat

In the RD model, electrical wavefronts regularly swept the lattice from top to bottom (Video S1, Figure 2A, top row). The entropy was relatively lower at the lattice borders and higher at the site of stimu-

lation, but these were artifacts of the boundary conditions and point stimulation, respectively (Figure 2B, top row). Otherwise, entropy was homogeneous across the lattice $[0.68 \text{ (mean)} \pm 0.03 \text{ (SD) bits}]$. Mutual information showed a spatially heterogeneous information sharing between cells (Figure 2C, top row) despite the assumed isotropic structure and homogeneous electrical properties of the lattice. For example, Figure 2C3 (top row) shows that the cell in the center of the lattice shares a high amount of information with the cells on the same electrical wavefront (yellow band) generated by the heartbeats. It also shows little information sharing with the cells preceding and following the wavefront (light blue bands surrounding the yellow band). This is clearly shown in the profile of mutual information (Figure 2D, top row) along the vertical broken line in Figure 2C3 (top row). Mutual information (red line) reached its peak (0.69 bits) at the center (profile position 64), where mutual information is equal to entropy because the mutual information of an entity with itself is equal to entropy (Equation 6). Mutual information fell off sharply from the center and reached the minimum (0 bits) on both sides (profile position 41 and 86) before slightly rising to approximately 0.06 bits on both ends. These findings indicate that the cells share a high amount of information when they are in phase with the cardiac excitation and share little information when they are out of phase. We formed an analytical framework which corroborates these numerical results (Appendix S1).

In the CA model (Video S2, Figure 2A, bottom row), the electrical wavefront was more irregular and unstable than that of the RD model. Entropy was homogeneous across the lattice, but was lower (0.52 ± 0.00 bits) than that of the RD model (Figure 2B, bottom row). This difference results from the fact that the CA model had a longer resting state (Video S2), making it more biased towards the resting state than the RD model (Video S1). There was no qualitative difference in information sharing between the RD model (Figure 2, top row) and the CA model (Figure 2, bottom row). However, information sharing was lower in the CA model because the CA model is inherently probabilistic and less reproducible than the RD model. The profile of mutual information (Figure 2D) along the vertical broken line in Figure 2C3 also shows a qualitatively similar but lower mutual information in the CA model (Figure 2D) relative to the RD model (Figure 2D).

Anatomical Reentry

In both the RD (Video S3) and the CA models (Video S4), the entropy of the cells within the circular non-excitable region was zero because these cells were always in the resting state (Figure 3A, B). The entropy was roughly homogeneous in other regions of the lattice. The average entropy was 0.32 ± 0.17 bits in the RD model and 0.69 ± 0.33 bits in the CA model (Figure 3B). The difference resulted from the longer wavelength in the CA model due to the more convex curvature than the RD model.

Overall, both models showed a similar spatial pattern of mutual information (Figure 3C). Information sharing between cells was spatially heterogeneous but showed rotational symmetry about the non-excitable region in the center. For example, Figure 3C1 shows that the cell in the left upper quadrant of the lattice shares a high amount of information with the cells on the same electrical wavefront (the orange band in the RD model and the yellow band in the CA model). Information sharing in the cells on the three other quadrants (Figure 3C2, 4 and 5) was rotationally symmetric with that of Figure 3C1. Importantly, there is no information sharing between the cell within the circular non-excitable region and any other cells in the lattice (Figure 3C3). This is logical from both the standpoints of electrophysiology and information theory. Of note, similar to normal heartbeat (Figure 2C), both models also showed little information sharing with the cells that preceded and followed the region of a high amount of shared information (light blue bands before and after the yellow band). These findings indicate that, similar to normal heartbeat, the cells share a high amount of information when they are in phase with cardiac excitation, and share little information when they are out of phase.

Spiral Reentry

In the RD model (Video S5, Figure 4A, top row), a single rotor with a resultant spiral reentry was simulated in the lattice. The entropy of each individual cell in this simulation shows an important finding with potential clinical significance. The left lower quadrant and both upper quadrants of the lattice exhibited homogeneous entropy (0.74 ± 0.04 bits), except for the borders of the lattice which is an artifact of boundary conditions (Figure 4B, top row). The red region in the right lower quadrant represents the higher entropy near the spiral tip (rotor) caused by the conduction velocity (CV) slowing near the rotor due to a pronounced wavefront curvature (Figure 4B, top row). This slowing of CV effectively caused longer cardiac excitations, making the cells in this region more biased towards the excited state than the rest of the cells in the lattice not directly affected by the rotor, boosting the entropy in this region. Within the red region is an L-shaped, light green, beadlike structure representing the lower entropy in the path of the drifting core of the spiral reentry around which the rotor revolved. This result suggests that the entropy of individual cells may be used to aid in localizing the core of spiral reentry for therapeutic purposes. Of note, the L-shaped path of the drifting core in this model was artificially determined by the boundary condition of the model.

While the entropy of individual cells provided very important findings, the average entropy over all cells was less informative. In fact, the average entropy between normal heartbeat and spiral reentry in the RD model was very similar (0.68 ± 0.03 *vs.* 0.74 ± 0.04 bits, respectively). This suggests that the spatial profiles of entropy are more useful in highlighting the difference in dynamics than the aggregate information over the entire tissue, as averaging effectively filters out the important features of the entropy landscape.

Mutual information was far more spatially heterogeneous than anticipated from the electrical wave propagation. For example, Figure 4C3 (top row) shows that the high level of information sharing in the central region of the lattice quickly faded as distance between cells increased. This reflects the fact that the cells lying along the same electrical wavefront changed over time due to the drifting core. This resulted in the smaller region of high information sharing in the spiral reentry than in normal heartbeat. This finding indicates that mutual information can sensitively detect regional heterogeneity of cardiac excitation in spiral reentry, which is not apparent from electrical wave propagation. Of note, information sharing in the right lower quadrant was limited to a focal region without a spiral tail (Figure 4C5, top row). This is because the cell in the right lower quadrant (green circle) happened to lie on the path of the drifting core, which coincided with a void of cardiac excitation.

In the CA model (Video S6, Figure 4A, bottom row), the electrical wavefront was inherently more irregular than that of the RD model. The entropy was roughly homogeneous across the lattice and close to 1 (0.97 ± 0.00 bits) (Figure 4B, bottom row). The higher entropy of the CA model compared with the RD model was, as in the anatomical reentry, caused by the longer wavelength in the CA model due to the more convex curvature than the RD model (Figure 4A, bottom row). Unlike the RD model, the entropy in the CA model did not show the path of the drifting core, indicating that the drift trajectory was much more random compared to that of the RD model with respect to the time frame (10 sec) of data acquisition. Information sharing between cells was spatially heterogeneous (Figure 4C, D) because of the regional heterogeneity of cardiac excitation in spiral reentry. Overall, the CA model showed lower information sharing than the RD model due to the probabilistic nature of the model.

Multiple Reentry

In both the RD (Video S7) and the CA models (Video S8), the entropy was homogeneous across the cell lattice (Figure 5A). The average entropy was 0.88 ± 0.03 bits in the RD model and 0.97 ± 0.00 bits in the CA model (Figure 5B). This indicates that excited and resting states are almost equally distributed throughout the time series of all the cells, yielding a high uncertainty and homogeneous entropy. The spatial profiles of information sharing for both the RD and the CA models were similar to

that of spiral reentry (Figure 5C), except the fact that the underlying structure was much less organized due to the random nature of multiple reentry. Information sharing was low except for a small region in the immediate neighborhood of the cell in which mutual information was measured. Outside this small region information sharing steeply fell off to near zero (Figure 5D). The near-zero mutual information indicates that the cells almost completely lost synchrony during multiple reentry; that is, individual cardiomyocytes got excited independently from each other and did not share information with cells beyond their immediate neighborhood.

Discussion

Summary of the Findings

By treating the heart as an electrical communication system, we demonstrated quantitatively that information sharing between cardiomyocytes on an isotropic lattice structure is spatially heterogeneous. This finding was unexpected from the traditional concept of the heart as a functional syncytium sharing electrical information via gap junctions, where one might mistakenly assume that information sharing would be homogeneous along the electrical wavefront. We also found that entropy can be significantly different between heart rhythms with electrically similar spatial patterns (Figure 2B, 4B and 3B). These findings indicate that metrics from information theory can quantitatively assess the communication processes within the heart which are not obvious from conventional electrocardiographic metrics such as sequences of electrical excitation. In addition, our results show that cardiac arrhythmia significantly impacts electrical communication within the heart.

Mutual Information to Quantify Communication Within the Heart

Analysis of dynamical multivariate data sets over the dimensions of time and physical space is commonly encountered in the investigation of complex systems [48]. The study of cardiac arrhythmia, particularly cardiac fibrillation, is no exception. For example, a number of measures to quantify spatial complexity of VF have been proposed, including the correlation length [49], the multiplicity index [50], and Karhunen-Loève decomposition [51]. The main focus of interest in these studies was to quantify the determinism and the predictability of the time series over physical space.

Our study is different from these previous studies in two aspects. First, our focus of interest was to quantify communication within the heart. Of central importance to the understanding of complex systems is connectivity, or the presence of dynamical interactions between spatially distinct locations within the system. Knowledge about connectivity in a system, whether anatomical or functional, further facilitates the fundamental understanding of the system since it addresses an important aspect of the functional interdependency of between each component of the system. Our results indicate that information theory metrics can quantitatively assess electrical communication processes among cardiomyocytes during normal heartbeat and complex arrhythmias beyond electrocardiographic measures, conferring validity to the paradigm of the heart as a communication system. Second, we used mutual information to perform spatial profiling of different cardiac arrhythmias. Correlations within multivariate time series can be described by measures such as linear and nonlinear correlation functions. However, mutual information has attracted considerable attention recently since it promises a very general quantification of statistical dependence [52]. In addition, previous studies measured the spatial profile of mutual information during VF [53], which could include both spiral reentry and multiple reentry, because it is challenging to distinguish one from the other in experimental settings. Therefore, the spatial profile of spiral reentry and multiple reentry was not clearly delineated. Our result showed that the spatial profile and the underlying structure of mutual information during each arrhythmia are clearly different (Figure 4 and 5). This suggests that information theory metrics may be able to help distinguish one rhythm from another by quantifying

communication within the heart.

The underlying mechanism of perturbation of information transfer during arrhythmia remains unclear. Information sharing during VF seems to be directly affected by the anisotropy of myofiber orientation and cell-to-cell coupling [53]. However, the spatial profile of membrane potential during VF has no consistent relationship with that of intracellular calcium dynamics [54]. This may suggest a contribution of non-voltage-gated intracellular calcium release in perturbation of information transfer by increasing the local complex interactions between calcium dynamics and membrane potential. Clearly, further studies will be needed to investigate the mechanistic basis of the paradigm of the heart as a communication system.

Clinical Implications

Recently, targeted elimination of the rotor (phase singularity) of spiral reentry has been shown to result in sustained termination of AF [55]. As a result, spatial localization of the rotor has attracted substantial attention in clinical cardiac electrophysiology. Entropy has been quantified to identify the location of the rotor of spiral reentry from the bipolar electrograms by creating the probability density function based on the amplitude of the signal [56]. However, the accuracy of this metric was not clear, because it has consistent correlation with complex fractionated electrograms [57], which was found to bear no spatial relevance to spiral reentry [58]. Therefore, the knowledge of the spatial profile of entropy for spiral reentry was lacking.

Our result in the RD model clearly showed that the region of rotor drift has high entropy (red region, right lower quadrant in Figure 4B, top row), which is consistent with the previous studies [56]. Moreover, what was most striking was the fact that entropy can localize the path of the drifting core of spiral reentry (L-shaped, light green, beadlike structure, right lower quadrant in Figure 4B, top row), because of the low entropy of the spiral core. This makes electrophysiological sense because the cardiomyocytes within the spiral core are almost constantly depolarized [59], making the probability density biased towards one. Therefore, our result showed a critically important fact that entropy can spatially localize the core (low entropy) within a larger region of the drifting rotor (high entropy). However, because a similar structure of the spatial profile could not be identified in the CA model (Figure 4B, bottom row), localization of the drifting core may require a spatially stable spiral reentry with adequately slow drift. Although these preliminary findings need to be confirmed in experimental models of cardiac fibrillation, they illustrate the potential clinical utility of information theory applied to cardiac electrophysiology.

Limitations

There are two limitations that should be considered before our results can be translated to human patients. First, the cardiac tissue was assumed to be a 2-D, isotropic, and homogeneous lattice, whereas real cardiac tissue is 3-D, anisotropic, and heterogeneous due to the intricately woven myofiber structure [60] and regional heterogeneity [61]. These tissue properties may contribute critically to the generation of cardiac arrhythmia [62]. However, the main focus of this work was to prove the concept that quantitative analysis of electrical communication during existing cardiac arrhythmia could yield clinically relevant results. We used two widely accepted models of action potential propagation in cardiac tissue to reproduce a variety of heart rhythms that captured important features of clinically representative arrhythmias. Therefore, we believe that these model assumptions were acceptable within the scope of this work. Second, our computation of information theory metrics did not incorporate conduction delay of electrical current to travel from one cell to another, since the time series of the entire lattice was acquired simultaneously. This is because the conduction delay within the small 2-D lattice would be negligibly small relative to the acquisition period of 10 seconds. However, this assumption may have underestimated the true amount of information sharing between heart cells because the standard definition of mutual information does not include shared information that is delayed in time. This leaves open the potential for even more clinically useful results by considering generalizations of the metric that explicitly account for this conduction delay.

Conclusions

Information theory metrics can quantitatively assess electrical communication processes among cardiomyocytes during normal heartbeat and complex arrhythmias beyond electrocardiographic measures. Further, entropy may have a clinical application in the localization and elimination of spiral reentry cores. These results suggest that the heart as a communication system is more complex than the traditional concept of functional syncytium sharing electrical information via gap junctions. We believe that this new paradigm provides a new set of tools for the systems-approach to the heart as a complex system [63].

Acknowledgments

This work was conducted as a research project during the Complex Systems Summer School at the Santa Fe Institute (SFI), NM, USA. The authors thank all the staff at SFI, particularly Sander Bais, Juniper Lovato, and John-Paul Gonzales. The authors also thank Felipe Alonso Atienza, Ferney Beltrán-Molina, Jesús Requena Carrión and Peter Hammer for generously providing the source code for the models described in the paper. The authors also thank Simon DeDeo and Nix Barnett for valuable input.

References

1. Kapoor N, Liang W, Marbán E, Cho HC. Direct conversion of quiescent cardiomyocytes to pacemaker cells by expression of Tbx18. *Nat Biotechnol.* 2013 Jan;31(1):54–62.
2. Hall JE. *Guyton and Hall Textbook of Medical Physiology*. 12th ed. Saunders; 2010.
3. Fishman GI, Spray DC, Levinwand LA. Molecular characterization and functional expression of the human cardiac gap junction channel. *J Cell Biol.* 1990 Aug;111(2):589–98.
4. Katz MD. *Physiology of the Heart*. 5th ed. Lippincott Williams and Wilkins; 2010.
5. Pertsov AM, Davidenko JM, Salomonsz R, Baxter WT, Jalife J. Spiral waves of excitation underlie reentrant activity in isolated cardiac muscle. *Circ Res.* 1993 Mar;72(3):631–50.
6. Weiss JN, Qu Z, Chen PS, Lin SF, Karagueuzian HS, Hayashi H, et al. The dynamics of cardiac fibrillation. *Circulation.* 2005 Aug;112(8):1232–40.
7. Ashikaga H, Sasano T, Dong J, Zviman MM, Evers R, Hopenfeld B, et al. Magnetic resonance-based anatomical analysis of scar-related ventricular tachycardia: implications for catheter ablation. *Circ Res.* 2007;101(9):939–47.
8. Stevenson WG, Wilber DJ, Natale A, Jackman WM, Marchlinski FE, Talbert T, et al. Irrigated radiofrequency catheter ablation guided by electroanatomic mapping for recurrent ventricular tachycardia after myocardial infarction: the multicenter thermocool ventricular tachycardia ablation trial. *Circulation.* 2008;118(25):2773–82.
9. Wang Y, Cuculich PS, Zhang J, Desouza KA, Vijayakumar R, Chen J, et al. Noninvasive electroanatomic mapping of human ventricular arrhythmias with electrocardiographic imaging. *Sci Transl Med.* 2011;3(98):98ra84.
10. de Ruyter van Steveninck RR, Lewen GD, Strong SP, Koberle R, Bialek W. Reproducibility and variability in neural spike trains. *Science.* 1997 Mar;275(5307):1805–8.
11. Ziv E, Nemenman I, Wiggins CH. Optimal signal processing in small stochastic biochemical networks. *PLoS One.* 2007;2(10):e1077.

12. Tkacik G, Callan CG Jr, Bialek W. Information flow and optimization in transcriptional regulation. *Proc Natl Acad Sci U S A*. 2008 Aug;105(34):12265–70.
13. Mehta P, Goyal S, Long T, Bassler BL, Wingreen NS. Information processing and signal integration in bacterial quorum sensing. *Mol Syst Biol*. 2009;5:325.
14. Fuller D, Chen W, Adler M, Groisman A, Levine H, Rappel WJ, et al. External and internal constraints on eukaryotic chemotaxis. *Proc Natl Acad Sci U S A*. 2010 May;107(21):9656–9.
15. Cheong R, Rhee A, Wang CJ, Nemenman I, Levchenko A. Information transduction capacity of noisy biochemical signaling networks. *Science*. 2011 Oct;334(6054):354–8.
16. Adami C. The use of information theory in evolutionary biology. *Ann N Y Acad Sci*. 2012 May;1256:49–65.
17. Stevenson WG, Khan H, Sager P, Saxon LA, Middlekauff HR, Natterson PD, et al. Identification of reentry circuit sites during catheter mapping and radiofrequency ablation of ventricular tachycardia late after myocardial infarction. *Circulation*. 1993;88(4 Pt 1):1647–70.
18. Gray RA, Pertsov AM, Jalife J. Spatial and temporal organization during cardiac fibrillation. *Nature*. 1998 Mar;392(6671):75–8.
19. Moe GK, Rheinboldt WC, Abildskov JA. A computer model of atrial fibrillation. *Am Heart J*. 1964 Feb;67:200–20.
20. Fitzhugh R. Impulses and Physiological States in Theoretical Models of Nerve Membrane. *Biophys J*. 1961 Jul;1(6):445–66.
21. Nagumo J, Animoto S, Yoshizawa S. An active pulse transmission line simulating nerve axon. *Proc Inst Radio Engineers*. 1962;50:2061–70.
22. Hodgkin AL, Huxley AF. A quantitative description of membrane current and its application to conduction and excitation in nerve. *J Physiol*. 1952;117:500–44.
23. Rogers JM, McCulloch AD. A collocation–Galerkin finite element model of cardiac action potential propagation. *IEEE Trans Biomed Eng*. 1994 Aug;41(8):743–57.
24. Plank G, Zhou L, Greenstein JL, Cortassa S, Winslow RL, O’Rourke B, et al. From mitochondrial ion channels to arrhythmias in the heart: computational techniques to bridge the spatio-temporal scales. *Philos Trans A Math Phys Eng Sci*. 2008 Sep;366(1879):3381–409.
25. Campbell SG, Howard E, Aguado-Sierra J, Coppola BA, Omens JH, Mulligan LJ, et al. Effect of transmurally heterogeneous myocyte excitation-contraction coupling on canine left ventricular electromechanics. *Exp Physiol*. 2009 May;94(5):541–52.
26. Bourgeois EB, Fast VG, Collins RL, Gladden JD, Rogers JM. Change in conduction velocity due to fiber curvature in cultured neonatal rat ventricular myocytes. *IEEE Trans Biomed Eng*. 2009 Mar;56(3):855–61.
27. Plank G, Burton RA, Hales P, Bishop M, Mansoori T, Bernabeu MO, et al. Generation of histologically representative models of the individual heart: tools and application. *Philos Transact A Math Phys Eng Sci*. 2009;367(1896):2257–92.
28. Chamakuri N, Kunisch K, Plank G. On boundary stimulation and optimal boundary control of the bidomain equations. *Math Biosci*. 2013 Oct;245(2):206–15.

29. Le TB, Sotiropoulos F. Fluid-structure interaction of an aortic heart valve prosthesis driven by an animated anatomic left ventricle. *J Comput Phys.* 2013 Jul;244:41–62.
30. Sovilj S, Magjarević R, Lovell NH, Dokos S. A simplified 3D model of whole heart electrical activity and 12-lead ECG generation. *Comput Math Methods Med.* 2013;2013:134208.
31. Alonso-Atienza F, Rojo-Alvarez JL, D Alvarez, Moscoso M, Garcia-Alberola A. Reconstruction of transmembrane currents using Support Vector machines and its application to endocardial mapping: A model study. In: *Computers in Cardiology*; 2007. p. 121–124.
32. Barquero-Perez O, Rojo-Alvarez JL, Requena-Carrión J, Alonso-Atienza F, Everss E, Goya-Esteban R, et al. Cardiac arrhythmia spectral analysis of electrogram signals using Fourier Organization Analysis. In: *Computers in Cardiology*; 2009. p. 333–336.
33. Beltran-Molina F, Munoz-Gomez A, Rodriguez A, Vinagre JJ, Requena-Carrion J. Effects of lead spatial resolution on the spectrum of cardiac signals: A simulation study. In: *Engineering in Medicine and Biology Society, EMBC, 2011 Annual International Conference of the IEEE*; 2011. p. 3800–3803.
34. Beltran-Molina F, Requena-Carrion J, Vaisanen J. Analysis of the effects of lead configuration on cardiac spectrum. In: *Computing in Cardiology*; 2012. p. 833–836.
35. Requena-Carrión J, Vaisanen J, Alonso-Atienza F, Rojo-Álvarez JL, Hyttinen J, Garcia-Alberola A. Comparison of the scope of true and integrated bipolar leads in implantable cardioverter defibrillators. In: *Computers in Cardiology*; 2007. p. 233–236.
36. Requena-Carrión J, Beltrán-Molina FA, Marques A, G. Relating the spectrum of cardiac signals to the spatiotemporal dynamics of cardiac sources. *Biomedical Signal Processing and Control.* 2013;8(6):935–944.
37. Requena-Carrión J, Väisänen J, Alonso-Atienza F, García-Alberola A, Ramos-López FJ, Rojo-Alvarez JL. Sensitivity and spatial resolution of transvenous leads in implantable cardioverter defibrillator. *IEEE Trans Biomed Eng.* 2009 Dec;56(12):2773–81.
38. Vaisanen J, Requena Carrion J, Hyttinen J. Effects of activation origin in the subcutaneous ECG with horizontal and vertical bipolar lead orientation. In: *Computers in Cardiology*; 2008. p. 357–360.
39. Vaisanen J, Requena-Carrión J, Alonso-Atienza F, Rojo-Alvarez JL, Hyttinen J. Analysing effects of implant dimensions on electrocardiograph: A modeling approach. In: *Computers in Cardiology*; 2007. p. 41–44.
40. Väisänen J, Requena-Carrión J, Alonso-Atienza F, Rojo-Alvarez JL, Malmivuo J, Hyttinen J. Contribution of the left anterior myocardium to the body surface potentials in case of apical ectopic beat. *Conf Proc IEEE Eng Med Biol Soc.* 2007;2007:931–4.
41. Alonso Atienza F, Requena Carrión J, García Alberola A, Rojo Álvarez JL, Sánchez Muñoz JJ, Martínez Sánchez J, et al. A probabilistic model of cardiac electrical activity based on a cellular automata system. *Rev Esp Cardiol (Engl Ed).* 2005 Jan;58(1):41–7.
42. Luo CH, Rudy Y. A model of the ventricular cardiac action potential. Depolarization, repolarization, and their interaction. *Circ Res.* 1991 Jun;68(6):1501–26.
43. Fogoros RN. *Electrophysiologic Testing.* 5th ed. Wiley-Blackwell; 2012.

44. 7. In: Jalife J, Delmar M, Anumonwo J, Berenfeld O, Kalifa J, editors. Rotors, spirals, and scroll waves in the heart. In: Basic Cardiac Electrophysiology for the Clinician. 2nd ed. Wiley-Blackwell, Oxford, UK; 2009. .
45. Calkins H, Kuck KH, Cappato R, Brugada J, Camm AJ, Chen SA, et al. 2012 HRS/EHRA/ECAS expert consensus statement on catheter and surgical ablation of atrial fibrillation. *Heart Rhythm*. 2012 Apr;9(4):632–696.e21.
46. Schotten U, Verheule S, Kirchhof P, Goette A. Pathophysiological mechanisms of atrial fibrillation: a translational appraisal. *Physiol Rev*. 2011 Jan;91(1):265–325.
47. Cover TM, Thomas JA. Elements of Information Theory. 2nd ed. Wiley-Interscience; 2006.
48. Galka A, Ozaki T, Bayard JB, Yamashita O. Whitening as a tool for estimating mutual information in spatiotemporal data sets. *J Stat Phys*. 2006;124:1275–315.
49. Bayly PV, Johnson EE, Wolf PD, Greenside HS, Smith WM, Ideker RE. A quantitative measurement of spatial order in ventricular fibrillation. *J Cardiovasc Electrophysiol*. 1993 Oct;4(5):533–46.
50. Rogers JM, Usui M, KenKnight BH, Ideker RE, Smith WM. Recurrent wavefront morphologies: a method for quantifying the complexity of epicardial activation patterns. *Ann Biomed Eng*. 1997;25(5):761–8.
51. Bayly PV, KenKnight BH, Rogers JM, Johnson EE, Ideker RE, Smith WM. Spatial organization, predictability, and determinism in ventricular fibrillation. *Chaos*. 1998 Mar;8(1):103–115.
52. Li W. Mutual information functions versus correlation functions. *J Stat Phys*. 1990;60:823–37.
53. Choi BR, Liu T, Lavasani M, Salama G. Fiber orientation and cell-cell coupling influence ventricular fibrillation dynamics. *J Cardiovasc Electrophysiol*. 2003 Aug;14(8):851–60.
54. Omichi C, Lamp ST, Lin SF, Yang J, Baher A, Zhou S, et al. Intracellular Ca dynamics in ventricular fibrillation. *Am J Physiol Heart Circ Physiol*. 2004 May;286(5):H1836–44.
55. Narayan SM, Krummen DE, Shivkumar K, Clopton P, Rappel WJ, Miller JM. Treatment of atrial fibrillation by the ablation of localized sources: CONFIRM (Conventional Ablation for Atrial Fibrillation With or Without Focal Impulse and Rotor Modulation) trial. *J Am Coll Cardiol*. 2012;60(7):628–36.
56. Ganesan AN, Kuklik P, Lau DH, Brooks AG, Baumert M, Lim WW, et al. Bipolar electrogram shannon entropy at sites of rotational activation: implications for ablation of atrial fibrillation. *Circ Arrhythm Electrophysiol*. 2013 Feb;6(1):48–57.
57. Ng J, Borodyanskiy AI, Chang ET, Villuendas R, Dibs S, Kadish AH, et al. Measuring the complexity of atrial fibrillation electrograms. *J Cardiovasc Electrophysiol*. 2010 Jun;21(6):649–55.
58. Narayan SM, Shivkumar K, Krummen DE, Miller JM, Rappel WJ. Panoramic electrophysiological mapping but not electrogram morphology identifies stable sources for human atrial fibrillation: stable atrial fibrillation rotors and focal sources relate poorly to fractionated electrograms. *Circ Arrhythm Electrophysiol*. 2013 Feb;6(1):58–67.
59. Qu Z, Kil J, Xie F, Garfinkel A, Weiss JN. Scroll wave dynamics in a three-dimensional cardiac tissue model: roles of restitution, thickness, and fiber rotation. *Biophys J*. 2000;78(6):2761–75.
60. Streeter J D D, Spotnitz HM, Patel DP, Ross J J, Sonnenblick EH. Fiber orientation in the canine left ventricle during diastole and systole. *Circ Res*. 1969;24(3):339–47.

61. Antzelevitch C, Fish J. Electrical heterogeneity within the ventricular wall. *Basic Res Cardiol*. 2001;96(6):517–27.
62. Qu Z, Xie F, Garfinkel A, Weiss JN. Origins of spiral wave meander and breakup in a two-dimensional cardiac tissue model. *Ann Biomed Eng*. 2000 Jul;28(7):755–71.
63. McCulloch AD, Paternostro G. Cardiac systems biology. *Ann N Y Acad Sci*. 2005 Jun;1047:283–95.
64. Shannon CE. A mathematical theory of communication. *Bell Syst Tech J*. 1948;27(379-423):623–656.

Figure Captions

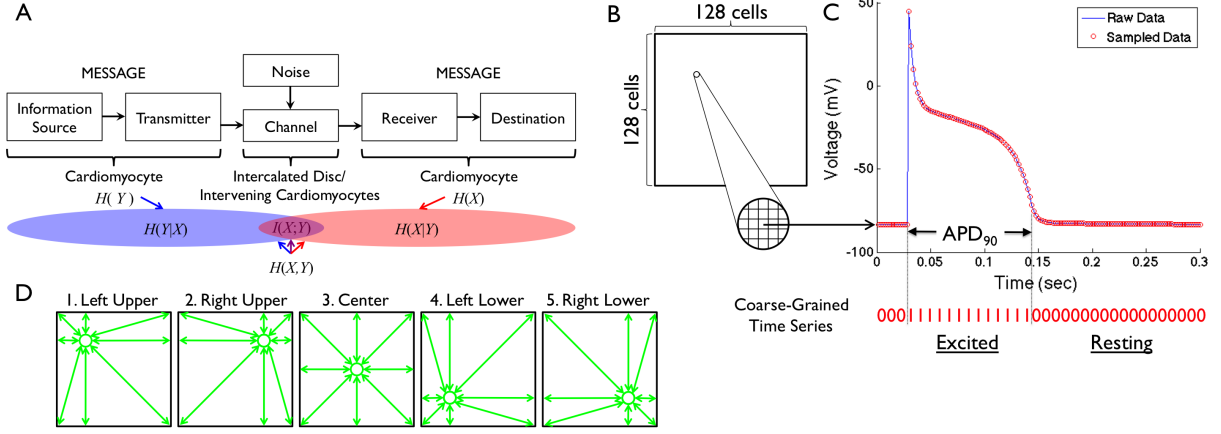


Figure 1. Conceptual Overview of the Methods. *A. The Heart as a Communication System.*

The heart can be considered as a communication system where cardiomyocytes act as an information source/transmitter and a receiver/destination with channels being intercalated discs/intervening cardiomyocytes. $H(X)$ and $H(Y)$ are the entropies of time series X and Y respectively; $H(X,Y)$ is the joint entropy of X and Y ; $H(X|Y)$ is the conditional entropy of X given Y ; $H(Y|X)$ is conditional entropy of Y given X ; $I(X;Y)$ is the mutual information of X and Y . Figure modified from [64]. *B. 2-D Lattice Model of Cardiac Tissue.* For both the reaction diffusion and the cellular automata models, the cardiac tissue was simulated as a 128 x 128 cell lattice, which was assumed to be isotropic. *C.*

Coarse-Graining of the Time Series. In each cell, the time series of cardiac excitation was computed for 10 seconds during four different heart rhythms (normal heartbeat, spiral reentry, anatomical reentry, and multiple reentry) at a sampling rate of 500/sec. The time series was coarse-grained to 1 when excited (during action potential duration at 90% repolarization APD₉₀) or 0 when resting. *D. Mutual Information.* To understand the spatial characteristics of information sharing among cardiomyocytes, mutual information was computed between five representative cells (green circles) and all the other cells in the 2-D lattice. These representative cells included cells in the left-upper quadrant (32,32), the right-upper quadrant (32,96), the center (64,64), the left-lower quadrant (96,32) and the right-lower quadrant (96,96).

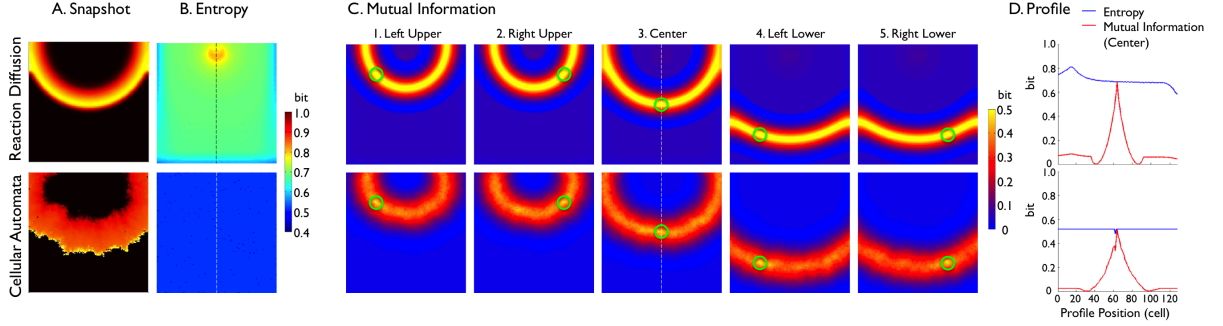


Figure 2. Normal Heartbeat. The top row represents the deterministic reaction diffusion (RD) model and the bottom row represents the probabilistic cellular automata (CA) model. *A. Snapshot of Electrical Wave Propagation* shows a representative snapshot of an electrical wave from Videos S1 (top) and S2 (bottom). *B. Entropy of Each Cell in the Cardiac Tissue* shows a heat map of the entropy in bits over the cell lattice. *C. Mutual Information Between Two Cells in the Cardiac Tissue* shows a heat map of mutual information in bits over the cell lattice. Mutual information was computed between a specific cell (green circle) and all the other cells in the same cardiac tissue. *D. Profiles of Entropy and Mutual Information* show profiles of entropy (blue line) and mutual information (red line) through the cell lattice along the vertical broken line shown in 2B and 2C3. Center, respectively.

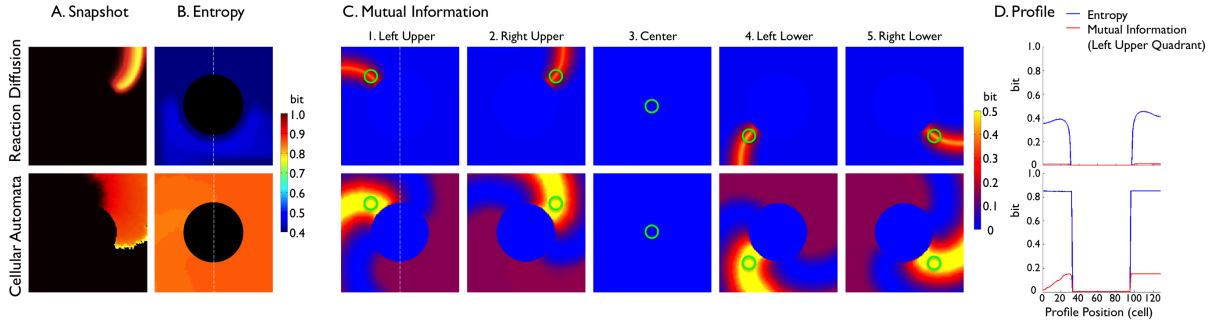


Figure 3. Anatomical Reentry. The black circular region in A and B represents a non-excitable tissue that serves as an anatomical obstacle around which cardiac excitation rotates perpetually. The top row represents the deterministic reaction-diffusion (RD) model and the bottom row represents the probabilistic cellular automata (CA) model. *A. Snapshot of Electrical Wave Propagation* shows a representative snapshot of an electrical wave from Videos S5 (top) and S6 (bottom). *B. Entropy of Each Cell in the Cardiac Tissue* shows a heat map of the entropy in bits over the cell lattice. *C. Mutual Information Between Two Cells in the Cardiac Tissue* shows a heat map of mutual information in bits over the cell lattice. Mutual information was computed between a specific cell (green circle) and all the other cells in the same cardiac tissue. *D. Profiles of Entropy and Mutual Information* shows the profile of entropy (blue line) through the cell lattice along the vertical broken line shown in 4B. The profile of mutual information (red line) in 4D is from 4C1. Left Upper Quadrant.

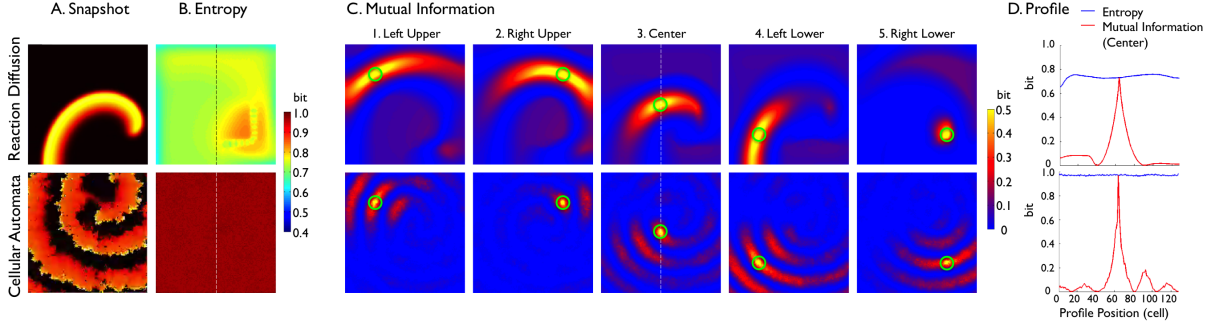


Figure 4. Spiral Reentry. The top row represents the deterministic reaction diffusion (RD) model and the bottom row represents the probabilistic cellular automata (CA) model. *A. Snapshot of Electrical Wave Propagation* shows a representative snapshot of an electrical wave from Videos S3 (top) and S4 (bottom). *B. Entropy of Each Cell in the Cardiac Tissue* shows a heat map of the entropy in bits over the cell lattice. *C. Mutual Information Between Two Cells in the Cardiac Tissue* shows a heat map of mutual information in bits over the cell lattice. Mutual information was computed between a specific cell (green circle) and all the other cells in the same cardiac tissue. *D. Profiles of Entropy and Mutual Information* show profiles of entropy (blue line) and mutual information (red line) through the cell lattice along the vertical broken line shown in 3B and 3C. Center, respectively.

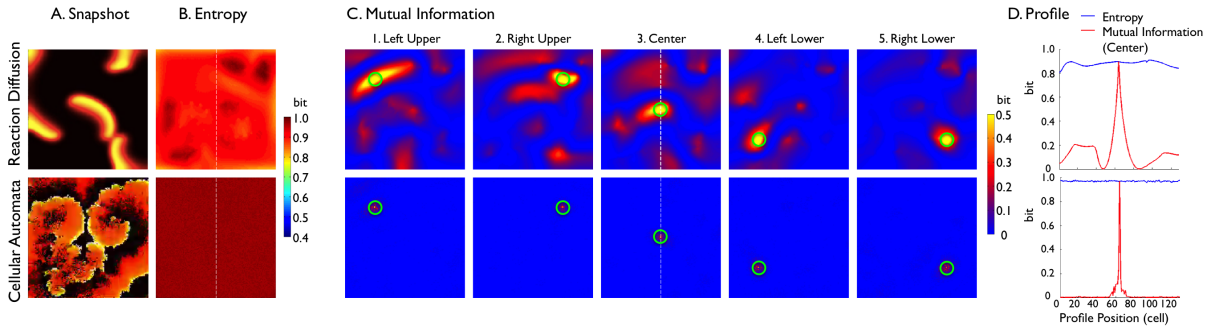


Figure 5. Multiple Reentry. The top row represents the deterministic reaction diffusion (RD) model and the bottom row represents the probabilistic cellular automata (CA) model. *A. Snapshot of Electrical Wave Propagation* shows a representative snapshot of an electrical wave from Videos S7 (top) and S8 (bottom). *B. Entropy of Each Cell in the Cardiac Tissue* shows a heat map of the entropy in bits over the cell lattice. *C. Mutual Information Between Two Cells in the Cardiac Tissue* shows a heat map of mutual information in bits over the cell lattice. Mutual information was computed between a specific cell (green circle) and all the other cells in the same cardiac tissue. *D. Profiles of Entropy and Mutual Information* show profiles of entropy (blue line) and mutual information (red line) through the cell lattice along the vertical broken line shown in 5B and 5C. Center, respectively.

Electronic Supplementary Materials

Video S1. Normal Heartbeat (Reaction Diffusion Model).
Video S2. Normal Heartbeat (Cellular Automata Model).
Video S3. Anatomical Reentry (Reaction Diffusion Model).
Video S4. Anatomical Reentry (Cellular Automata Model).
Video S5. Spiral Reentry (Reaction Diffusion Model).
Video S6. Spiral Reentry (Cellular Automata Model).
Video S7. Multiple Reentry (Reaction Diffusion Model).
Video S8. Multiple Reentry (Cellular Automata Model).
Appendix S1. Sensitivity Analysis of Mutual Information in Cardiac Tissue.

Short Title For Page Headings

The Heart as a Communication System

Electronic Supplementary Material for
Modeling the Heart as a Communication System

Hiroshi Ashikaga*, José Aguilar-Rodríguez, Shai Gorsky, Elizabeth Lusczek, Flávia Maria Darcie Marquitti, Brian Thompson, Degang Wu, Joshua Garland

*To whom correspondence should be addressed. E-mail: hashika1@jhmi.edu

Appendix S1. Sensitivity Analysis of Mutual Information in Cardiac Tissue

In this section, we build an analytical model to determine the sensitivity of mutual information to each parameter of the cardiac tissue using a simple model of unidirectional plane wave propagation. The analytical result should help the reader understand the numerical results in the paper.

Basic Cardiac Electrophysiology

The cardiac tissue is simulated as a 2-dimensional (2-D), isotropic lattice of an arbitrary size (FigureS1), where a vertical plane wave of excitation emerges from the left edge of the tissue at a constant inter-beat interval (basic cycle length, BCL), and travels toward the right edge with conduction velocity CV .

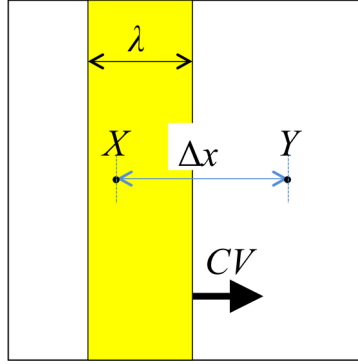


Figure S1. A 2-D Isotropic Excitable Tissue of an Arbitrary Size. A vertical plane wave of excitation (in yellow) emerges from the left edge of the tissue, travels toward the right edge with conduction velocity CV . λ is the wavelength of the excitation wave. Δx is the horizontal distance between two arbitrary points X and Y on the cardiac tissue.

We define the BCL in terms of the diastolic interval DI and the action potential duration APD (FigureS2A):

$$BCL = DI_{i+1} + APD_i \quad (1)$$

where i is the beat number. In this analysis, we assume that APD is determined only by the immediately preceding DI (APD restitution) [1]:

$$APD_i = f(DI_i) \quad (2)$$

Other factors could influence APD in more complex models [2].

When BCL is constant and the slope of the restitution curve at the fixed point denoted by the asterisk (*) is less than one, that is, $df/dDI < 1$, APD and DI converge to constant values (FigureS2B). Therefore, the solution to the restitution function at a steady state is

$$APD = f(DI) \quad (3)$$

Similar to APD , CV in cardiac tissue is a function of the preceding DI and tends to decrease monotonically as DI decreases [3].

$$CV_i = g(DI_i) \quad (4)$$

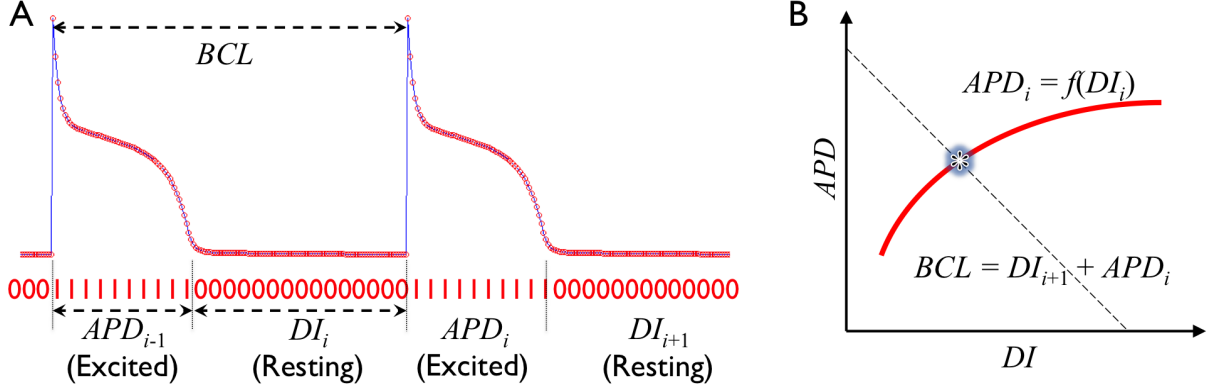


Figure S2. Action Potential Duration (APD) Restitution. *A. Basic cycle length (BCL).* BCL is the inter-beat interval. APD is the action potential duration and DI is the diastolic interval, where $BCL = DI_{i+1} + APD_i$. i denotes the beat number. In our study the time series at each point in the cardiac tissue was coarse-grained to 1 during APD (= excited) or 0 during DI (= resting). *B. APD restitution curve.* APD is a function of the immediately preceding DI ($APD_i = f(DI_i)$). The dashed line represents $BCL = DI_{i+1} + APD_i$. The asterisk (*) denotes the stable fixed point when BCL is constant and the slope of the restitution curve at the fixed point is less than one.

CV is highest for fully recovered tissue, and there is a minimum DI for propagation at a finite CV. APD and CV are related by the wavelength of the excitation wave λ :

$$\lambda = APD \times CV \quad (5)$$

Mutual Information in Cardiac Tissue

At time $t = 0$, the point X in Figure S1 is resting. The point X becomes excited when the plane wave of excitation reaches the point X . Therefore, the electrophysiological behaviors of point X over time can be described using a square wave (Figure S3). The point X remains excited while the plane wave travels from left to right at the conduction velocity CV. From Equation 5, the duration of excitement is

$$\frac{\lambda}{CV} = APD \quad (6)$$

When $\Delta x \geq \lambda$, the joint probability distribution $p(x, y)$ at the points X and Y is

$$\begin{aligned} p(X = 1, Y = 0) &= p(X = 0, Y = 1) = \frac{APD}{BCL} = \frac{APD}{APD + DI} = \frac{1}{1 + \frac{DI}{APD}} = \frac{1}{1 + \frac{DI}{f(DI)}} \\ p(X = 1, Y = 1) &= 0 \\ p(X = 0, Y = 0) &= 1 - \frac{2APD}{BCL} = 1 - \frac{2}{1 + \frac{DI}{f(DI)}} \end{aligned}$$

The marginal probabilities $p(x)$ and $p(y)$ at the points X and Y are

$$\begin{aligned} p(X = 1) &= p(Y = 1) = \frac{APD}{BCL} = \frac{1}{1 + \frac{DI}{f(DI)}} \\ p(X = 0) &= p(Y = 0) = 1 - \frac{APD}{BCL} = 1 - \frac{1}{1 + \frac{DI}{f(DI)}} \end{aligned}$$

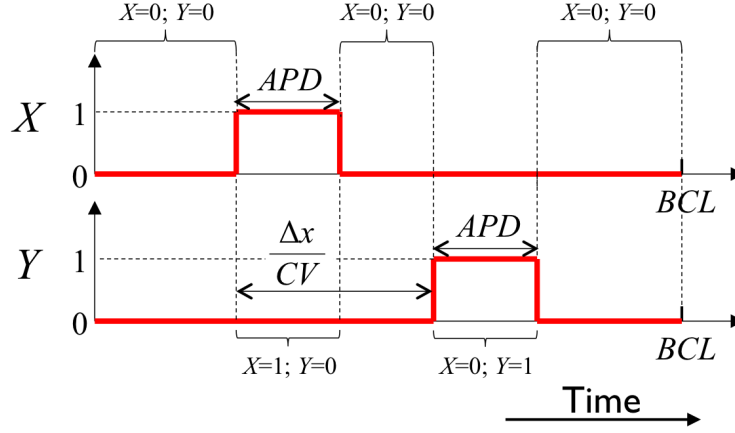


Figure S3. Electrophysiological Behaviors of Two Arbitrary Points X and Y in Figure S1. This figure illustrates the case where $\Delta x \geq \lambda$, but a similar analysis can be conducted in the case of $\Delta x < \lambda$. The values 0 and 1 represent the 'resting' and 'excited' states, respectively. At $t = 0$, the point X is resting. When the plane wave of excitation reaches the point X at the conduction velocity CV it becomes excited, remains excited for the duration of APD (action potential duration), then becomes resting again. The point Y, which is located Δx distal to the point X with respect to the wave propagation, becomes excited $\Delta x/CV$ after the point X becomes excited. The duration of excitation at the point Y is also APD . This time sequence repeats itself at the rate of BCL (basic cycle length).

Mutual information $I(X;Y)$ is defined as [4]

$$I(X;Y) = \sum_{x,y} p(x,y) \log_2 \frac{p(x,y)}{p(x)p(y)} \quad (7)$$

If we define a new variable l such that

$$l = \frac{APD}{BCL} = \frac{\lambda}{CV \times BCL} = \frac{1}{1 + \frac{DI}{f(DI)}} \quad (8)$$

then the joint probability distribution $p(x,y)$ and the marginal probabilities $p(x)$ and $p(y)$ are

$$\begin{aligned} p(X = 1, Y = 0) &= p(X = 0, Y = 1) = l \\ p(X = 1, Y = 1) &= 0 \\ p(X = 0, Y = 0) &= 1 - 2l \\ p(X = 1) &= p(Y = 1) = l \\ p(X = 0) &= p(Y = 0) = 1 - l \end{aligned}$$

Note that l is dependent only on DI . From Equation 7, mutual information $I(X;Y)$ is

$$\begin{aligned} I(X;Y) &= p(X = 1, Y = 0) \log_2 \frac{p(X = 1, Y = 0)}{p(X = 1)p(Y = 0)} + p(X = 0, Y = 1) \log_2 \frac{p(X = 0, Y = 1)}{p(X = 0)p(Y = 1)} \\ &\quad + p(X = 1, Y = 1) \log_2 \frac{p(X = 1, Y = 1)}{p(X = 1)p(Y = 1)} + p(X = 0, Y = 0) \log_2 \frac{p(X = 0, Y = 0)}{p(X = 0)p(Y = 0)} \\ &= l \log_2 \frac{l}{l(1-l)} + l \log_2 \frac{l}{l(1-l)} + 0 + (1-2l) \log_2 \frac{1-2l}{(1-l)^2} \\ &= -2(1-l) \log_2(1-l) + (1-2l) \log_2(1-2l) \end{aligned} \quad (9)$$

We define a new variable d such that

$$d = \frac{\frac{\Delta x}{CV}}{BCL} = \frac{\Delta x}{CV \times BCL} = \frac{\Delta x}{g(DI) [f(DI) + DI]} \quad (10)$$

Note d is dependent only on DI and Δx . When $\Delta x < \lambda$, the joint probability distribution $p(x, y)$ and the marginal probabilities $p(x)$ and $p(y)$ are

$$\begin{aligned} p(X = 1, Y = 0) &= p(X = 0, Y = 1) = \frac{\frac{\Delta x}{CV}}{BCL} = d \\ p(X = 1, Y = 1) &= \frac{APD - \frac{\Delta x}{CV}}{BCL} = l - d \\ p(X = 0, Y = 0) &= 1 - \frac{APD + \frac{\Delta x}{CV}}{BCL} = 1 - l - d \\ p(X = 1) &= p(Y = 1) = l \\ p(X = 0) &= p(Y = 0) = 1 - l \end{aligned}$$

Therefore, mutual information $I(X; Y)$ is

$$\begin{aligned} I(X; Y) &= p(X = 1, Y = 0) \log_2 \frac{p(X = 1, Y = 0)}{p(X = 1)p(Y = 0)} + p(X = 0, Y = 1) \log_2 \frac{p(X = 0, Y = 1)}{p(X = 0)p(Y = 1)} \\ &\quad + p(X = 1, Y = 1) \log_2 \frac{p(X = 1, Y = 1)}{p(X = 1)p(Y = 1)} + p(X = 0, Y = 0) \log_2 \frac{p(X = 0, Y = 0)}{p(X = 0)p(Y = 0)} \\ &= d \log_2 \frac{d}{l(1-l)} + d \log_2 \frac{d}{l(1-l)} + (l-d) \log_2 \frac{l-d}{l^2} + (1-l-d) \log_2 \frac{1-l-d}{(1-l)^2} \\ &= 2d \log_2 d - 2l \log_2 l - 2(1-l) \log_2(1-l) + (l-d) \log_2(l-d) + (1-l-d) \log_2(1-l-d) \end{aligned} \quad (11)$$

To summarize,

$$I(X; Y) = \begin{cases} 2(l-1) \log(1-l) + (1-2l) \log(1-2l) & d \geq l \\ 2d \log_2 d - 2l \log_2 l - 2(1-l) \log_2(1-l) + (l-d) \log_2(l-d) + (1-l-d) \log_2(1-l-d) & d < l \end{cases}$$

From Equation 9 and 11, as DI increases, both l and d decrease. Accordingly, the mutual information between two arbitrary points at a distance d becomes smaller (Figure S4). This sensitivity of mutual information to DI accounts for the lower average information sharing in the normal heartbeats in the cellular automata model compared to the reaction diffusion model in Figure 6 in the main paper. Figure S4 also illustrates the phenomenon of little information sharing when the two points are out of phase that is shown in the normal heartbeats in Figure 2 in the main paper.

References

1. Nolasco JB, Dahlen RW. A graphic method for the study of alternation in cardiac action potentials. J Appl Physiol. 1968 Aug;25(2):191–6.
2. Berger RD. Electrical restitution hysteresis: good memory or delayed response? Circ Res. 2004 Mar;94(5):567–9.
3. Gray RA. 34. In: Zipes DP, Jalife J, editors. Theory of rotors and arrhythmias. In Cardiac Electrophysiology: From Cell to Bedside. 6th ed. Saunders; 2014. p. 191–223.
4. Cover TM, Thomas JA. Elements of Information Theory. 2nd ed. Wiley-Interscience; 2006.

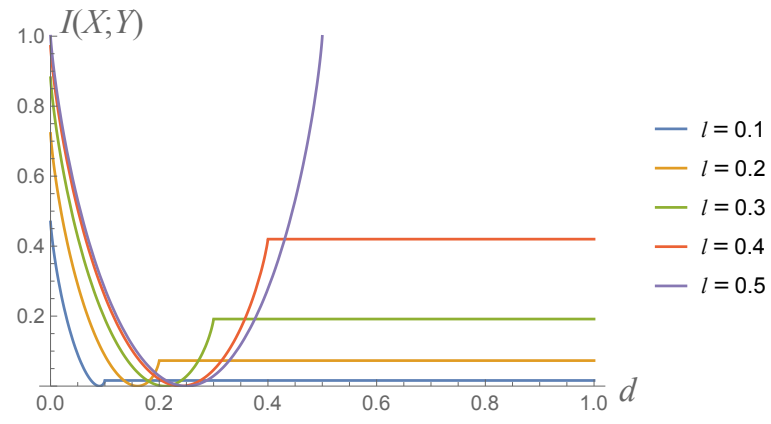


Figure S4. Mutual Information Between Two Arbitrary Points as a Function of d and l .